

Effects of two gaps and paramagnetic pair breaking on the upper critical field of $\text{SmFeAsO}_{0.85}$ and $\text{SmFeAsO}_{0.8}\text{F}_{0.2}$ single crystals

Hyun-Sook Lee,¹ Marek Bartkowiak,² Jae-Hyun Park,¹ Jae-Yeap Lee,¹ Ju-Young Kim,³ Nak-Heon Sung,³ B. K. Cho,³ Chang-Uk Jung,⁴ Jun Sung Kim,¹ and Hu-Jong Lee^{1,*}

¹*Department of Physics, Pohang University of Science and Technology, Pohang 790-784, Republic of Korea*

²*Hochfeld-Magnetlabor Dresden (HLD), Forschungszentrum Dresden-Rossendorf, D-01314 Dresden, Germany*

³*Department of Materials Science and Engineering, GIST, Gwangju 500-712, Republic of Korea*

⁴*Department of Physics, Hankuk University of Foreign Studies, Yongin, Gyeonggi 449-791, Republic of Korea*

(Received 29 July 2009; revised manuscript received 18 September 2009; published 9 October 2009)

We investigated the temperature dependence of the upper critical field [$H_{c2}(T)$] of fluorine-free $\text{SmFeAsO}_{0.85}$ and fluorine-doped $\text{SmFeAsO}_{0.8}\text{F}_{0.2}$ single crystals by measuring the resistive transition in low static magnetic fields and in pulsed fields up to 60 T. Both crystals show that $H_{c2}(T)$'s along the c axis [$H_{c2}^c(T)$] and in an ab -planar direction [$H_{c2}^{ab}(T)$] exhibit a linear and a sublinear increase, respectively, with decreasing temperature below the superconducting transition. $H_{c2}(T)$'s in both directions deviate from the conventional one-gap Werthamer-Helfand-Hohenberg theoretical prediction at low temperatures. A two-gap nature and the paramagnetic pair-breaking effect are shown to be responsible for the temperature-dependent behavior of H_{c2}^c and H_{c2}^{ab} , respectively.

DOI: 10.1103/PhysRevB.80.144512

PACS number(s): 74.25.Fy, 74.25.Op, 74.70.-b

I. INTRODUCTION

The upper critical field, H_{c2} , is one of the most important superconducting parameters, providing a valuable insight into the pairing mechanism and information on fundamental superconducting properties such as coherence length scales. The temperature dependence of the upper critical field $H_{c2}(T)$ and its anisotropy are sensitive to the details of the underlying electronic structures and reflect the dimensionality of superconductivity. Furthermore, H_{c2} is related to the critical current density, which is an important material parameter for application purposes.

After the discovery of iron-pnictides-based superconductors,¹ $RE\text{FeAsO}_{1-x}\text{F}_x$ (RE =rare-earth elements), with relatively high-superconducting transition temperature (T_c), many efforts have been made to investigate their $H_{c2}(T)$. $RE\text{FeAsO}_{1-x}\text{F}_x$ has a layered structure with alternating stacks of insulating REO and conducting FeAs layers. Despite the presence of the two-dimensional nature in the materials, most of studies on $H_{c2}(T)$ of $RE\text{FeAsO}_{1-x}\text{F}_x$ have been limited to polycrystals^{2,3} because of the difficulty with growing $RE\text{FeAsO}_{1-x}\text{F}_x$ single crystals. Therefore, recent investigations of single crystals have been more focused on $A\text{EFe}_2\text{As}_2$ ($A\text{E}$ =alkaline-earth elements) (Refs. 4–6) single crystals, which can be grown with relative ease in the ambient conditions. High-field measurements on electron- and hole-doped $A\text{EFe}_2\text{As}_2$ single crystals and films^{7–11} showed that $H_{c2}(T)$ in a c -axis field [$H_{c2}^c(T)$] and in an ab -planar field [$H_{c2}^{ab}(T)$] increases almost linearly and sublinearly with decreasing temperature below T_c , respectively, regardless of the doping level and the degree of disorder. The resultant $H_{c2}^{ab}(T)$ approaches the value of $H_{c2}^c(T)$ at T far below T_c , leading to the almost isotropic superconductivity in the zero-temperature limit. Such a quasi-isotropic property of $H_{c2}(T)$ in a layered structure is quite intriguing and has been attributed to the multiband effect.^{9–11}

Recently single crystalline $RE\text{FeAsO}_{1-x}\text{F}_x$ (RE =Sm, Nd, and Pr) (Refs. 12–15) were successfully grown by using the

flux-growth technique or the high-pressure high-temperature technique. There is, however, a single report on the $H_{c2}(T)$ of $RE\text{FeAsO}_{1-x}\text{F}_x$ single crystals for $\text{NdFeAsO}_{0.7}\text{F}_{0.3}$ at temperatures far below T_c , where $H_{c2}(T)$ was traced by high-field resistivity measurements using pulsed magnetic field up to 60 T.¹⁶ $H_{c2}^c(T)$ in the study exhibited a pronounced upturn curvature at low temperatures.¹⁶ By contrast, $H_{c2}^{ab}(T)$ showed a downturn curvature in the low-temperature range.¹⁶ Apparently, the temperature dependence of H_{c2}^c for $\text{NdFeAsO}_{1-x}\text{F}_x$, despite being common iron-arsenic compounds, appears to be quite different from that of $A\text{EFe}_2\text{As}_2$. Thus, it is highly required to examine any common or dissimilar $H_{c2}(T)$ behavior of different compounds of $RE\text{FeAsO}_{1-x}\text{F}_x$, both in c -axis and in ab -planar fields, by adopting high-quality single crystals.

In this paper, we present $H_{c2}(T)$ for the magnetic fields along the c axis ($H_{\parallel c}$) and in the ab plane ($H_{\parallel ab}$) for single crystals of oxygen-deficient $\text{SmFeAsO}_{0.85}$ and fluorine-doped $\text{SmFeAsO}_{0.8}\text{F}_{0.2}$. $H_{c2}(T)$ were determined from the resistive transition in pulsed (static) magnetic fields up to 60 T (6.9 T). The sublinear increase in $H_{c2}^{ab}(T)$ with decreasing temperature below T_c , as previously seen in a $\text{NdFeAsO}_{0.7}\text{F}_{0.3}$ single crystal¹⁶ and in $A\text{EFe}_2\text{As}_2$ compounds,^{7–11} was also observed in our crystals. On the other hand, $H_{c2}^c(T)$'s of our $\text{SmFeAsO}_{0.85}$ and $\text{SmFeAsO}_{0.8}\text{F}_{0.2}$ crystals linearly increase with decreasing temperature near T_c but tend to be saturated far below T_c . This temperature dependence of H_{c2}^c is in contrast to the linear temperature dependence found in $A\text{EFe}_2\text{As}_2$ in all the temperature range below T_c (Refs. 7–11) and to the significant upturn behavior in $\text{NdFeAsO}_{0.7}\text{F}_{0.3}$ single crystals below T_c .¹⁶ A deviation of $H_{c2}(T)$ from the conventional one-gap Werthamer-Helfand-Hohenberg (WHH) prediction is found in our crystals. This feature, along with the reduction in its anisotropy with lowering temperatures, turns out to be common to iron-pnictides superconductors. Its detailed temperature dependence and the anisotropy, however, can be quite different depending on the

compounds, which indicates the complex interplay of a multiband nature and the paramagnetic effect.

II. EXPERIMENT

Single crystals of $\text{SmFeAsO}_{0.85}$ and $\text{SmFeAsO}_{0.8}\text{F}_{0.2}$ with nominal compositions were grown using the self-flux method under high-temperature and high-pressure condition. Stoichiometric starting compounds of SmAs, Fe_2O_3 , and Fe for $\text{SmFeAsO}_{0.85}$ single crystals and SmAs, FeAs, Fe_2O_3 , Fe, and SmF_3 for $\text{SmFeAsO}_{0.8}\text{F}_{0.2}$ single crystals were used. A pellet sealed in a boron-nitride container was placed in a cubic pyrophyllite cell equipped with a carbon heater. A 14 mm cubic multianvil-type press was used to pressurize the whole assembly. Heat treatment at 1350–1450 °C was done for 8–10 h under a constant pressure of 3.3 GPa, which was then followed by rapid cooling to room temperature. Details of the single-crystal growth are described elsewhere.¹⁷ After the pressure was released, the final bulk was mechanically crushed to separate the single crystals from the flux.

Thus-grown crystals have platelike shapes. X-ray diffraction reveals that the crystal surface is normal to the c axis with the plate-shaped surface along the ab plane. In-plane resistive transition of $\text{SmFeAsO}_{0.85}$ and $\text{SmFeAsO}_{0.8}\text{F}_{0.2}$ single crystals was measured using the standard four-probe technique. Contact leads were prepared by using photolithography on the platelike sample surface. The upper insets of Figs. 1(a) and 1(b) show optical microscopic images of the four-probe patterned $\text{SmFeAsO}_{0.85}$ (dimensions: $\sim 80 \times 50 \times 10 \mu\text{m}^3$) and $\text{SmFeAsO}_{0.8}\text{F}_{0.2}$ (dimensions: $\sim 60 \times 50 \times 10 \mu\text{m}^3$) single-crystal specimens, respectively. The contact resistance of each lead was $\sim 1 \Omega$. The resistive transition [$R(T)$] was measured in low applied magnetic fields up to 6.9 T. Resistance as a function of fields [$R(H)$] up to 60 T was also measured at different temperatures in pulsed-field facilities at Hochfeld-Magnetlabor Dresden. During the measurements, magnetic fields were applied along the c axis and in the ab plane while maintaining the current flow of 1 mA normal to the magnetic field, for which the heating due to the contact and the sample resistance was negligible.

III. RESULTS

As shown in the lower insets of Figs. 1(a) and 1(b), the superconducting transitions in zero field are very sharp for both $\text{SmFeAsO}_{0.85}$ and $\text{SmFeAsO}_{0.8}\text{F}_{0.2}$ crystals. The onset of the superconducting transition, defined by the deviation from the linear $R(T)$ above T_c , occurs at about $T_{c,\text{onset}} = 50.5$ K for $\text{SmFeAsO}_{0.85}$ and about 42 K for $\text{SmFeAsO}_{0.8}\text{F}_{0.2}$. The transition width ΔT_c , determined by adopting the criterion of 10–90 % of the normal-state resistance R_n , is ~ 0.5 K for $\text{SmFeAsO}_{0.85}$ and ~ 0.8 K for $\text{SmFeAsO}_{0.8}\text{F}_{0.2}$. ΔT_c 's for both crystals are much narrower than the reported values of 2–4 K for single crystalline $\text{REFeAsO}_{1-x}\text{F}_x$ ($\text{RE} = \text{Sm}$ and Nd),^{14,15,18} indicating good quality of our samples. As Figs. 1(a) and 1(b) show, the residual resistivity ratio (RRR), $\text{RRR} \equiv \rho(300 \text{ K}) / \rho(T_{c,\text{onset}})$ of ~ 4.5 for $\text{SmFeAsO}_{0.85}$ is larger than the value of 2.5 seen

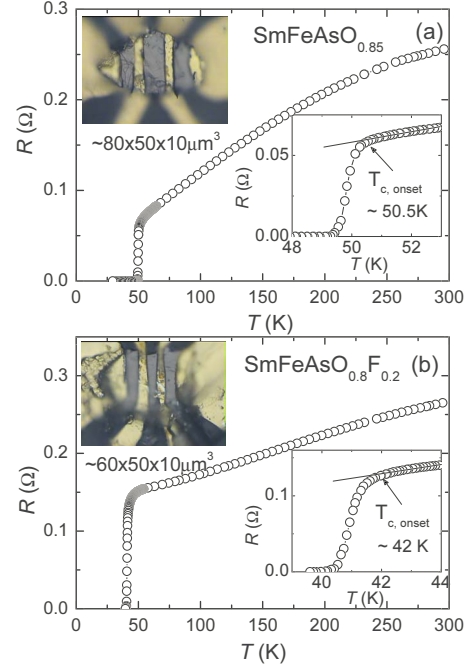


FIG. 1. (Color online) Temperature dependence of the resistance $R(T)$ of (a) $\text{SmFeAsO}_{0.85}$ and (b) $\text{SmFeAsO}_{0.8}\text{F}_{0.2}$ single crystals in zero magnetic field. The upper insets of (a) and (b) show the microscopic images of the four-probe patterned crystals used for the transport measurements. The lower insets of (a) and (b) show a magnified view near the superconducting transition. The onset of superconducting transition, $T_{c,\text{onset}}$, defined by the deviation from the linearity of $R(T)$, is indicated in the lower insets.

previously for $\text{NdFeAsO}_{0.82}\text{F}_{0.18}$ single crystals,^{14,18} while RRR of $\text{SmFeAsO}_{0.8}\text{F}_{0.2}$ is ~ 2.2 , which is somewhat smaller but still comparable to that of the previous report. This indicates that the impurity scattering effect in our fluorine-free $\text{SmFeAsO}_{0.85}$ single crystal is less than the fluorine-doped $\text{REFeAsO}_{1-x}\text{F}_x$ single crystal. According to the recent report,¹⁹ fluorine does not fully substitute for oxygen and, thus, some oxygen vacancies remain in the crystal. The resulting additional scattering centers in $\text{REFeAsO}_{1-x}\text{F}_x$ may have enhanced the impurity scattering and led to a smaller RRR value than in SmFeAsO_{1-x} .

Figures 2(a) and 2(b) present temperature dependence of resistance [$R(T)$] of $\text{SmFeAsO}_{0.85}$ single crystal in low magnetic fields from 0 to 6.9 T for $H_{\parallel c}$ and $H_{\parallel ab}$, respectively. The corresponding $R(T)$ of $\text{SmFeAsO}_{0.8}\text{F}_{0.2}$ single crystal is displayed in Figs. 3(a) and 3(b). Upon increasing magnetic fields, the resistive transition in $H_{\parallel c}$ becomes broader and the onset of superconductivity shifts to lower temperatures. The trend is more conspicuous in $H_{\parallel c}$ than in $H_{\parallel ab}$. These behaviors of $R(T)$ in low magnetic fields of $H_{\parallel c}$ and $H_{\parallel ab}$ in both crystals are similar to what was previously reported for $\text{SmFeAsO}_{0.7}\text{F}_{0.25}$ (Ref. 15) and $\text{NdFeAsO}_{0.82}\text{F}_{0.18}$ (Refs. 14 and 16) single crystals. However, details of the magnetic-field dependence are notably different from the previous observation. In our crystals, the resistive tail is more clearly observed for $H_{\parallel c}$, in particular, with a gradual extension to lower temperatures with increasing fields [see Fig. 2(a) for $\text{SmFeAsO}_{0.85}$ and Fig. 3(a) for $\text{SmFeAsO}_{0.8}\text{F}_{0.2}$]. The tail of

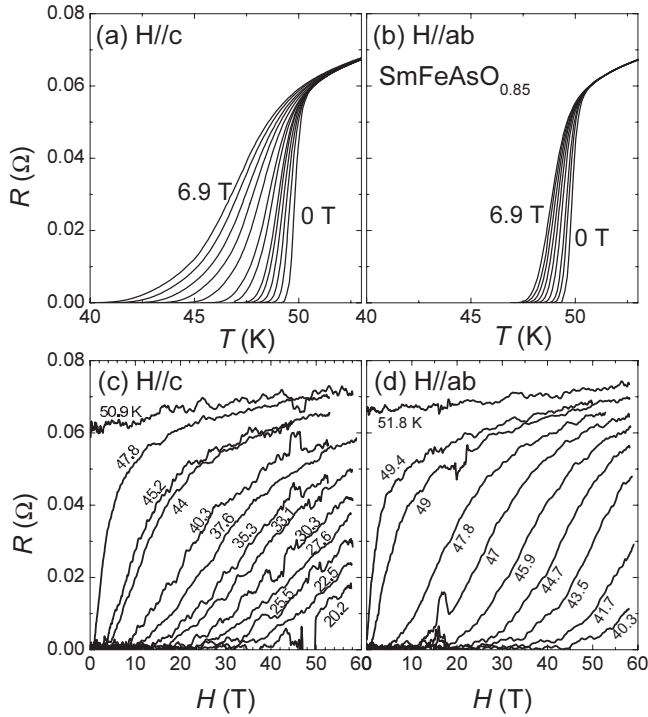


FIG. 2. Temperature dependence of the resistance $R(T)$ of $\text{SmFeAsO}_{0.85}$ single crystal measured at the various static fields from 0 to 6.9 T for (a) $H_{\parallel c}$ (0, 0.2, 0.4, 0.6, 0.8, 1, 1.5, 2, 3, 4, 5, 6, and 6.9 T) and (b) $H_{\parallel ab}$ (0, 0.5, 1, 2, 3, 4, 5, 6, and 6.9 T). Field dependence of the resistance $R(H)$ of $\text{SmFeAsO}_{0.85}$ single crystal measured at various temperatures in pulsed magnetic fields up to 60 T for (c) $H_{\parallel c}$ and (d) $H_{\parallel ab}$.

$R(T)$ was also observed in high $H_{\parallel c}$ in cuprates^{20–23} and in $\text{YNi}_2\text{B}_2\text{C}$,²⁴ where both have layered structure with CuO_2 and Ni_2B_2 conducting planes, respectively. It has been known that such a resistive tail can be explained in terms of the vortex-glass phase.²⁵ Therefore, the observation of the $R(T)$ tail in our crystals indicates the possible formation of the vortex-glass phase for $H > 2$ T. In the same magnetic-field region of $H_{\parallel c}$, the formation of vortex-liquid phase was also confirmed in $\text{NdFeAsO}_{1-x}\text{F}_x$ single crystals.²⁶ Oxygen vacancies in both of our $\text{SmFeAsO}_{0.85}$ and $\text{SmFeAsO}_{0.8}\text{F}_{0.2}$ crystals may have acted as random intrinsic point defects and induced the vortex-glass state. Detailed analysis on the vortex dynamics in our crystals will be presented separately.²⁷

The magnetic-field dependence of resistance [$R(H)$] of our $\text{SmFeAsO}_{0.85}$ [Figs. 2(c) and 2(d)] and $\text{SmFeAsO}_{0.8}\text{F}_{0.2}$ [Figs. 3(c) and 3(d)] crystals was measured in pulsed magnetic fields (both $H_{\parallel c}$ and $H_{\parallel ab}$) up to 60 T at various temperatures. The upper critical fields, H_{c2}^c for $H_{\parallel c}$ and H_{c2}^{ab} for $H_{\parallel ab}$, were obtained by adopting different criteria; 90%, 50%, and 10% of R_n . The normal-state resistance R_n was determined by linearly extrapolating the normal-state behavior above the onset of superconductivity in $R(T)$ and $R(H)$ curves separately. Thus-determined values of H_{c2}^c and H_{c2}^{ab} are shown in Figs. 4(a) and 4(b) for $\text{SmFeAsO}_{0.85}$ [in Figs. 4(c) and 4(d) for $\text{SmFeAsO}_{0.8}\text{F}_{0.2}$]. In both crystals, $H_{c2}(T)$ obtained from $R(T)$ (in Figs. 2 and 3) at low static magnetic fields (open symbols) is inline with those from $R(H)$ curves (in Figs. 2 and 3) at high pulsed magnetic fields (solid sym-

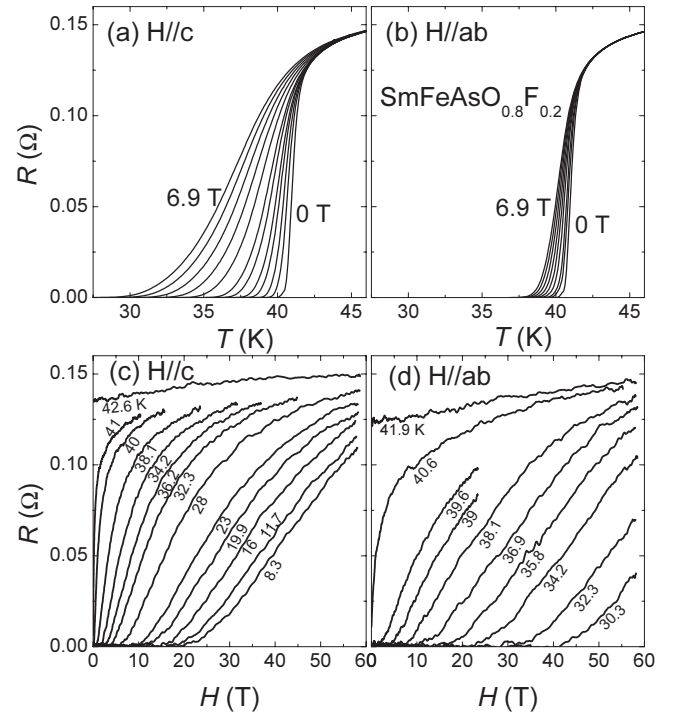


FIG. 3. Temperature dependence of the resistance $R(T)$ of $\text{SmFeAsO}_{0.8}\text{F}_{0.2}$ single crystal measured in the various static fields from 0 to 6.9 T for (a) $H_{\parallel c}$ (0, 0.2, 0.4, 0.7, 1, 1.5, 2, 3, 4, 5, 6, and 6.9 T) and (b) $H_{\parallel ab}$ (0, 0.5, 1, 2, 3, 4, 5, 6, and 6.9 T). Field dependence of the resistance $R(H)$ of $\text{SmFeAsO}_{0.8}\text{F}_{0.2}$ single crystal measured at various temperatures in pulsed magnetic fields up to 60 T for (c) $H_{\parallel c}$ and (d) $H_{\parallel ab}$.

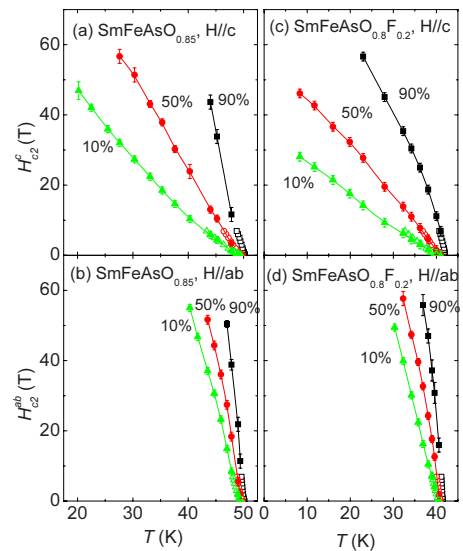


FIG. 4. (Color online) Temperature dependence of the upper critical fields $H_{c2}(T)$ of $\text{SmFeAsO}_{0.85}$ for (a) $H_{\parallel c}$ and (b) $H_{\parallel ab}$ and of $\text{SmFeAsO}_{0.8}\text{F}_{0.2}$ for (c) $H_{\parallel c}$ and (d) $H_{\parallel ab}$. $H_{c2}(T)$ values are extracted from 10%, 50%, and 90% of the normal-state resistance R_n determined by the linear extrapolation above the onset of superconductivity of $R(T)$ (open symbols) and of $R(H)$ (closed symbols) curves.

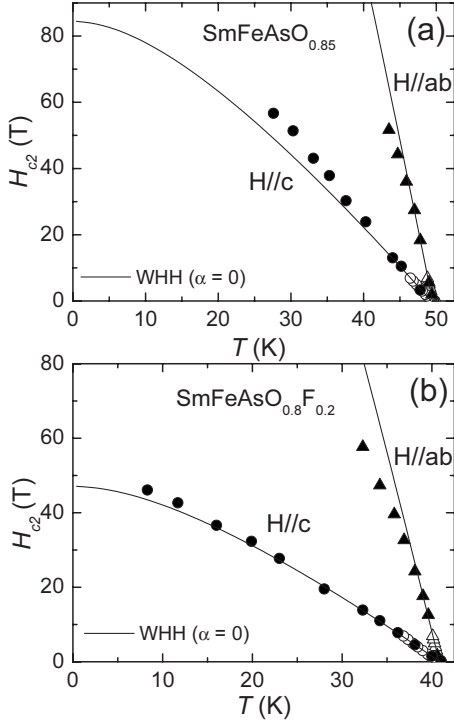


FIG. 5. $H_{c2}(T)$ for $H_{||c}$ (circles) and $H_{||ab}$ (triangles) of (a) $\text{SmFeAsO}_{0.85}$ and (b) $\text{SmFeAsO}_{0.8}\text{F}_{0.2}$ extracted from 50% of R_n shown in Figs. 4(a)–4(d). The open and closed symbols indicate the values of $H_{c2}(T)$ obtained from $R(T)$ and $R(H)$ curves, respectively. The experimental data were analyzed in terms of the WHH theory, which is exhibited by solid lines without the spin-paramagnetic effect ($\alpha=0$).

bols). With lowering temperature, $H_{c2}^c(T)$ exhibits a slight upturn variation for the 10% criteria but it turns gradually into a slight downturn curvature as one moves to 90% criteria, in particular, for $\text{SmFeAsO}_{0.8}\text{F}_{0.2}$ sample. Similar behavior has also been observed in cuprates.^{28–32} The criteria-dependent discrepancy arises from the fact that the region near 10% of R_n is related to the vortex-liquid phase while the region near 90% of R_n is affected by the superconducting fluctuation.^{29–32} Thus, we adopt the 50%- R_n criterion to determine $H_{c2}(T)$. The resultant $H_{c2}(T)$ for $H_{||c}$ and $H_{||ab}$ is summarized in Fig. 5(a) for $\text{SmFeAsO}_{0.85}$ [in Fig. 5(b) for $\text{SmFeAsO}_{0.8}\text{F}_{0.2}$]. The values of $H_{c2}(T)$ for $H_{||c}$ and $H_{||ab}$ of our $\text{SmFeAsO}_{0.85}$ and $\text{SmFeAsO}_{0.8}\text{F}_{0.2}$ single crystals are in

the same range as reported for the corresponding polycrystals, with the similar value of $T_c \sim 50$ and ~ 40 K, respectively, for the two crystals.^{3,33}

According to a recent report on high-field resistivity measurements in a $\text{NdFeAsO}_{0.7}\text{F}_{0.3}$ single crystal up to 60 T,¹⁶ $H_{c2}(T)$ for $H_{||c}$ exhibits a pronounced upturn in the entire ranges of magnetic field 60 T and temperature below $T_c \sim 45$ K. This result is similar to the earlier report for polycrystalline samples,^{2,3} where the upturn shape of $H_{c2}^c(T)$ was suggested to be an intrinsic property of iron pnictides and was explained in terms of the two-band model.^{2,3,16} However, our $\text{SmFeAsO}_{0.85}$ and $\text{SmFeAsO}_{0.8}\text{F}_{0.2}$ single crystals show linear increase in $H_{c2}^c(T)$ with decreasing temperature near T_c but tend to be saturated far below T_c [see Figs. 5(a) and 5(b)]. This temperature dependence of H_{c2}^c is in contrast to the linear and upturn temperature dependences in AEFe_2As_2 (Refs. 7–11) and in $\text{NdFeAsO}_{0.7}\text{F}_{0.3}$ single crystals,¹⁶ respectively, below T_c .

IV. DISCUSSION

First, we compare the $H_{c2}(T)$ data of our crystals with the conventional WHH theory,³⁴ which is based on the orbital effect arising from the Lorentz force acting on paired electrons with opposite momenta as the main cause of pair breaking. In addition, the theory is extended to include the effects of spin paramagnetism (α) and spin-orbit scattering (λ_{so}). Here, we assume that the spin-orbit scattering due to impurities is negligible ($\lambda_{so}=0$).³⁵ As shown in the Fig. 5, the data points of $H_{c2}(T)$ for $H_{||c}$ and $H_{||ab}$ in both crystals do not well follow the WHH model for $\alpha=0$ (solid lines). $H_{c2}^c(T)$'s for both crystals are enhanced compared to the WHH prediction while $H_{c2}^{ab}(T)$'s are suppressed below the WHH curve with a flattening behavior.

Using the WHH theory for $\alpha=0$ and $\lambda_{so}=0$, we estimate the H_{c2} value at $T=0$ [$H_{c2,\text{WHH}}(0)$]. $H_{c2,\text{WHH}}^c(0) \approx 84$ T (47 T) and $H_{c2,\text{WHH}}^{ab}(0) \approx 378$ T (280 T) for $\text{SmFeAsO}_{0.85}$ [$\text{SmFeAsO}_{0.8}\text{F}_{0.2}$] are obtained using the relation, $H_{c2,\text{WHH}}(0) = 0.69T_c |dH_{c2}/dT|_{T_c}$. The values of $|dH_{c2}/dT|_{T_c}$ are presented in Table I. It is noteworthy to compare these $H_{c2,\text{WHH}}(0)$ values with the paramagnetic limiting field due to Zeeman paramagnetic pair breaking, $H_p(T=0) \equiv (1 + \lambda_{ep})H_p^{\text{BCS}}(T=0)$. Here, $H_p^{\text{BCS}}(T=0) = 1.84T_c(H=0)$ (Ref. 36) is the Pauli or Clongston-Chandrasekhar-limit field

TABLE I. Superconducting parameters of $\text{SmFeAsO}_{0.85}$ and $\text{SmFeAsO}_{0.8}\text{F}_{0.2}$ single crystals obtained from the analysis of $H_{c2}(T)$. The c axis and the ab -plane coherence length, $\xi_c(0)$ and $\xi_{ab}(0)$, respectively, are estimated with the Ginzburg-Landau relations for the upper critical field of $H_{c2}^c = \Phi_0/2\pi\xi_{ab}^2(0)$ and $H_{c2}^{ab} = \Phi_0/2\pi\xi_{ab}(0)\xi_c(0)$.

	$T_{c,\text{onset}}$ (K)	$\left \frac{dH_{c2}}{dT} \right _{T_{c c}}$ (T/K)	$\left \frac{dH_{c2}}{dT} \right _{T_{c ab}}$ (T/K)	$H_{c2}^c(0)$ ^a (T)	$H_{c2}^{ab}(0)$ ^b (T)	$\xi_{ab}(0)$ (Å)	$\xi_c(0)$ (Å)
$\text{SmFeAsO}_{0.85}$	50.5	2.5	11	110	150	17	3.6
$\text{SmFeAsO}_{0.8}\text{F}_{0.2}$	42	1.7	9.9	50	100	26	3.6

^a $H_{c2}^c(0)$ is determined from the analysis with two-band model.

^b $H_{c2}^{ab}(0) \equiv H_{c2,\text{WHH}}^{ab}(T=0)$ is estimated with the WHH theory including paramagnetism.

for isotropic s -wave pairing in the absence of spin-orbit scattering in weakly coupled superconductors. λ_{ep} is introduced to take into account the strong electron-boson (i.e., phonon) coupling in the system. If we take^{16,35,37} $\lambda_{ep}=0.6$, $H_p(0)$'s for $\text{SmFeAsO}_{0.85}$ and $\text{SmFeAsO}_{0.8}\text{F}_{0.2}$ are estimated to be about 145 and 120 T, respectively. In both crystals, the values of $H_{c2,\text{WHH}}^c(0)$ are much smaller than the corresponding values of $H_p(0)$. This indicates that the H_{c2}^c is determined dominantly by the orbital effect rather than the paramagnetic effect. By contrast, $H_{c2,\text{WHH}}^{ab}(0)$ is much larger than $H_p(0)$. In fact, the $H_{c2}^c(T)$'s of both crystals have a tendency to be suppressed below the WHH curve for $\alpha=0$ and thus the actual $H_{c2}^c(0)$ is expected to be much smaller than $H_{c2,\text{WHH}}^c(0)$ estimated based on the paramagnetic effect. For $H_{c2}^c(T)$ where the orbital effect is dominant, on the other hand, its enhancement compared to the WHH curve with $\alpha=0$ cannot be explained in terms of the conventional one-gap WHH theory.

In order to understand the detailed temperature dependence of $H_{c2}^c(T)$, we consider the multiband nature of iron pnictides. It has been well known that there are two different coexisting groups of Fermi surfaces: one with electron and the other with hole character.^{38–42} Using the two-gap dirty-limit model of $H_{c2}(T)$ (Ref. 43) we can fit the experimental data as shown in Figs. 6(a) and 6(b). The equation of $H_{c2}(T)$ for $H_{\parallel c}$ considering orbital pair breaking is given by $a_0[\ln t + U(h)][\ln t + U(\eta h)] + a_2[\ln t + U(\eta h)] + a_1[\ln t + U(h)] = 0$, where $t = T/T_c$, $U(x) = \Psi(1/2 + x) - \Psi(x)$, $\Psi(x)$ is the Euler digamma function, $\eta = D_2/D_1$, $D_{1,2}$ are diffusivities of the bands 1 and 2, and $h = H_{c2}D_1/(2\phi_0T)$. $a_{0,1,2}$ are constants described with intraband- and interband-coupling constants $\lambda_{11,22}$ and $\lambda_{12,21}$ in the bands 1 and 2, respectively. Precise definitions of $a_{0,1,2}$ can be found in Ref. 43. The equation of $H_{c2}(T)$ can be generalized to the case of a field inclined by angle θ with respect to the ab plane by adopting angle-dependent diffusivities, $D_{1,2}(\theta) = [(D_{1,2}^{ab})^2 \cos^2 \theta + D_{1,2}^{ab} D_{1,2}^c \sin^2 \theta]^{1/2}$.⁴³ Therefore, $D_{1,2}$ are given by $D_{1,2}^{ab}$ for $H_{\parallel c}$ and $[D_{1,2}^{ab} D_{1,2}^c]^{1/2}$ for $H_{\parallel ab}$, where $D_{1,2}^{ab}$ ($D_{1,2}^c$) are the in-plane (out-of-plane) electron diffusivities of the bands 1 and 2. We discuss two different cases; (1) dominant intraband coupling $w > 0$ and (2) dominant interband coupling $w < 0$, where $w = \lambda_{11}\lambda_{22} - \lambda_{12}\lambda_{21}$. Here, we take three sets of λ for $w > 0$ [(1) $\lambda_{11}=0.8$, $\lambda_{22}=0.3$, and $\lambda_{12,21}=0.18$, (2) $\lambda_{11,22}=0.5$ and $\lambda_{12,21}=0.25$, (3) $\lambda_{11,22}=0.7$ and $\lambda_{12,21}=0.5$] and two sets of λ for $w < 0$ [(4) $\lambda_{11,22}=0.49$ and $\lambda_{12,21}=0.5$, (5) $\lambda_{11,22}=0.5$ and $\lambda_{12,21}=0.55$]. Due to the lack of microscopic theory of pairing mechanism, we choose the values of λ close to the ones adopted in earlier reports.^{2,9,16}

First, we consider the case of $H_{\parallel c}$. As shown in Fig. 6(a) for $\text{SmFeAsO}_{0.85}$, the $H_{c2}^c(T)$ predicted by the two-gap theory can reproduce nicely the experimental data taken up to 60 T for all cases. Depending on the sign of w , however, the theoretical curves have different curvatures beyond the field range of measurements. Near $T=0$, the H_{c2}^c curves saturate to the values of $H_{c2}^c(0) \sim 110$ T for (1) and ~ 135 –142 T for (2) and (3) in $w > 0$, but still rapidly increase with upturn curvatures toward $H_{c2}^c(0) \sim 220$ –300 T for (4) and (5) in $w < 0$. In these cases, $\eta_{\parallel c} = D_2^{ab}/D_1^{ab}$ is in the range of ~ 5 –9 for $w > 0$ and ~ 19 –36 for $w < 0$. In contrast, for

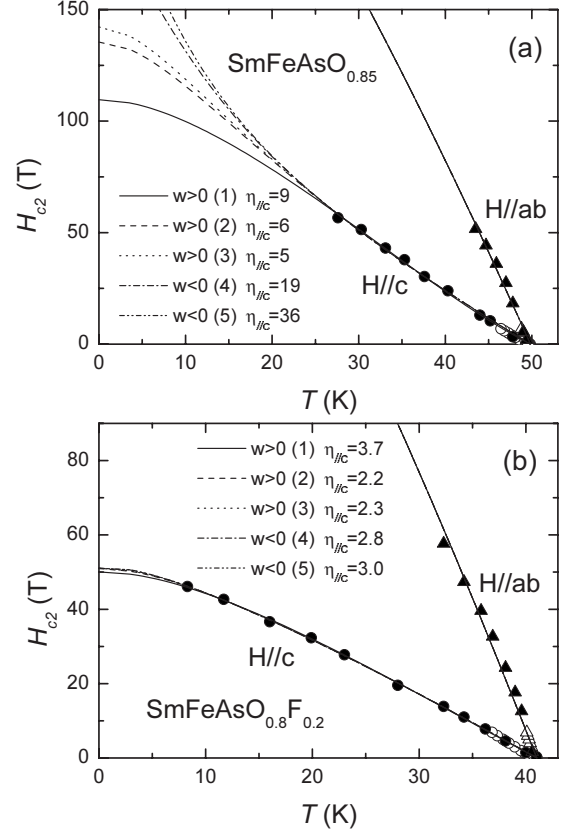


FIG. 6. Analysis of $H_{c2}(T)$ for $H_{\parallel c}$ and $H_{\parallel ab}$ of (a) $\text{SmFeAsO}_{0.85}$ and (b) $\text{SmFeAsO}_{0.8}\text{F}_{0.2}$ single crystals using the two-gap theory in different pairing scenario: for $w > 0$, (1) $\lambda_{11}=0.8$, $\lambda_{22}=0.3$, and $\lambda_{12,21}=0.18$, (2) $\lambda_{11,22}=0.5$ and $\lambda_{12,21}=0.25$, and (3) $\lambda_{11,22}=0.7$ and $\lambda_{12,21}=0.5$, and for $w < 0$, (4) $\lambda_{11,22}=0.49$ and $\lambda_{12,21}=0.5$, and (5) $\lambda_{11,22}=0.5$ and $\lambda_{12,21}=0.55$, where $w = \lambda_{11}\lambda_{22} - \lambda_{12}\lambda_{21}$. The best fit is obtained for different values of $\eta_{\parallel c} = D_2^{ab}/D_1^{ab}$ in the inset and an identical value of $\eta_{\parallel ab} = [D_2^{ab}D_2^c/D_1^{ab}D_1^c]^{1/2} = 1$.

$\text{SmFeAsO}_{0.8}\text{F}_{0.2}$, the different sets of fitting parameters lead to almost identical curves, well fitting the $H_{c2}^c(T)$ data [Fig. 6(b)] with $H_{c2}^c(0) \sim 50$ T, $H_{c2}^{ab}(0) \sim 208$ T, and $\eta_{\parallel c} \sim 2.2$ –3.7. This indeterminacy of the sign of w for a better fit to the H_{c2}^c of $\text{SmFeAsO}_{0.8}\text{F}_{0.2}$ may stem from the higher inhomogeneity of the crystal.

If we take into account the difference in the average Fermi velocities⁴⁴ of hole and electron sheets, the difference in the intraband diffusivities $D_2^{ab} \sim (19-36)D_1^{ab}$ for $w < 0$ looks too high. In addition, since $H_p(0) \sim 145$ T was estimated for $\text{SmFeAsO}_{0.85}$, the parameter set of (1) for $w > 0$, which gives $H_{c2}^c(0) \sim 110$ T, is more reasonable to explain the experimental data. Thus, in the reasonable range of $\eta_{\parallel c}$, the $H_{c2}^c(T)$ curves of both crystals do not show the pronounced upturn behavior in the whole field and temperature range. This is somewhat different from the result¹⁶ of $\text{NdFeAsO}_{0.7}\text{F}_{0.3}$ single crystal, showing the significant upturn of $H_{c2}^c(T)$ at the field up to 60 T. In Ref. 16, such a pronounced upturn of $H_{c2}^c(T)$ is explained in terms of a two-band model, assuming a large difference in D_2^{ab} and D_1^{ab} with $\eta_{\parallel c} \sim 10$ –100. It is not clear yet whether such a huge difference in D_2^{ab} and D_1^{ab} is intrinsic. As pointed out in Ref. 16 the strong upturn in $H_{c2}^c(T)$ can be due to scatterings at magnetic

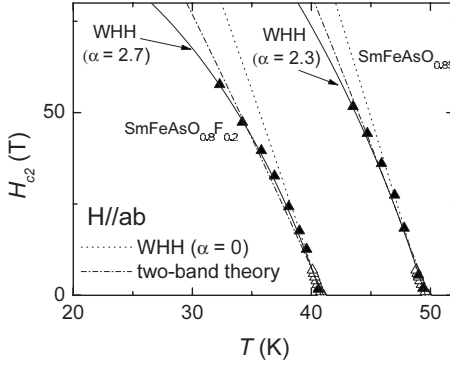


FIG. 7. Analysis of $H_{c2}(T)$ for $H_{||ab}$ by using the WHH theory including spin-paramagnetic effect ($\alpha \neq 0$). The flattening of $H_{c2}(T)$ for $H_{||ab}$ of $\text{SmFeAsO}_{0.85}$ and $\text{SmFeAsO}_{0.8}\text{F}_{0.2}$ single crystals, which can be clearly observed by a deviation from the dotted lines of the WHH theory for $\alpha=0$, is well explained by the WHH theory for $\alpha=2.3$ and 2.7 (solid lines), respectively, rather than by the two-band model (dash-dotted lines).

impurities. In any case, the strong deviation from the WHH model is a common feature of iron pnictides, which reflects the multigap nature of the materials.

Next, we consider the case of $H_{||ab}$. In both crystals, the various sets of fitting parameters using the two-gap model lead to an identical curve of $H_{c2}(T)$. As shown in Figs. 6(a) and 6(b), the fitting curves of two-band model cannot capture the flattening behavior with decreasing temperatures in both crystals. As discussed above, for $H_{||ab}$ we expect that the paramagnetic limiting³⁵ plays an essential role for determining $H_{c2}^{ab}(T)$. In the framework of the WHH theory, such a spin-paramagnetic effect can be taken into account by introducing the so-called Maki parameter, α . With $\alpha=2.3$ and 2.7 , the $H_{c2}^{ab}(T)$ data of $\text{SmFeAsO}_{0.85}$ and $\text{SmFeAsO}_{0.8}\text{F}_{0.2}$ crystals are nicely fitted by the WHH model (see Fig. 7). It has been known that the Maki parameter α becomes larger as the system is disordered.³⁵ A slightly larger value of α for $\text{SmFeAsO}_{0.8}\text{F}_{0.2}$ than for $\text{SmFeAsO}_{0.85}$ is consistent with its smaller RRR value. The values of $H_{c2, \text{WHH}}^p(0)$ obtained by considering the Pauli paramagnetism with $\alpha \neq 0$ in the WHH theory are estimated to be ≈ 150 T for $\text{SmFeAsO}_{0.85}$ and ≈ 100 T for $\text{SmFeAsO}_{0.8}\text{F}_{0.2}$. Since $H_{c2, \text{WHH}}^p(0) \geq H_p(0)$ in our crystals, the data of $H_{c2}^{ab}(T)$ are strongly affected by the spin paramagnetic effect rather than by the two-band nature.

Due to the quasi-two-dimensional Fermi-surface topology, for a $H_{||c}$, the cross section of the Fermi surface produces closed current loops that form vortices.^{45–49} Thus, for $H_{||c}$, the orbital pair-breaking mechanism plays a dominant role in destroying the superconductivity in high magnetic fields. Thus, the two-gap theory, taking into account the orbital pair-breaking effect, well describes our $H_{c2}^c(T)$ data. For a $H_{||ab}$, however, closed loops cannot be easily formed because the cross-sectional area of the Fermi surface is almost fully open⁵⁰ with negligible orbital effect, thus resulting in a rapid increase in $H_{c2}(T)$ near T_c . Therefore, the spin-paramagnetic effect is a more dominant factor in reducing the increase rate of $H_{c2}^{ab}(T)$ with decreasing temperature in our crystals.

In Fig. 8, the anisotropy of H_{c2} , $\gamma \equiv H_{c2}^{ab}/H_{c2}^c$, is plotted as

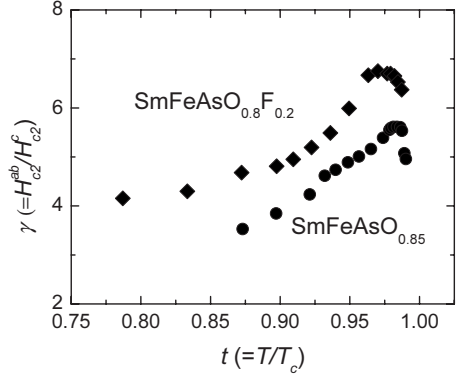


FIG. 8. Anisotropy ratio of H_{c2} , $\gamma \equiv H_{c2}^{ab}/H_{c2}^c$, as a function of reduced temperature $t = T/T_c$ for $\text{SmFeAsO}_{0.85}$ (circles) and $\text{SmFeAsO}_{0.8}\text{F}_{0.2}$ (diamonds) single crystals.

a function of reduced temperature $t = T/T_c$ for $\text{SmFeAsO}_{0.85}$ (circles) and $\text{SmFeAsO}_{0.8}\text{F}_{0.2}$ (diamonds). The value of γ for $\text{SmFeAsO}_{0.85}$ ($\text{SmFeAsO}_{0.8}\text{F}_{0.2}$) crystal is in the range of about 3–6 (4–7), at the temperature region of $T = (0.75–1)T_c$. $\text{SmFeAsO}_{0.8}\text{F}_{0.2}$ has a somewhat larger γ than $\text{SmFeAsO}_{0.85}$. These values are similar in magnitude to the ones reported in other $\text{REFeAsO}_{1-x}\text{F}_x$ ($\text{RE} = \text{Sm}$ and Nd) single crystals.^{14–16,18,51,52} The γ has temperature dependence, which is distinct from that of the conventional single-band superconductivity. The decreasing γ with decreasing temperature in both crystals results from the enhanced $H_{c2}^c(T)$ and the suppressed $H_{c2}^{ab}(T)$ compared to the WHH for $\alpha=0$ as shown in Figs. 5(a) and 5(b).⁵³ Therefore, the temperature dependence of γ originates from the combined effect of two-band nature and spin paramagnetism.

V. SUMMARY

This study reports on $H_{c2}^c(T)$ and $H_{c2}^{ab}(T)$ of fluorine-free $\text{SmFeAsO}_{0.85}$ and fluorine-doped $\text{SmFeAsO}_{0.8}\text{F}_{0.2}$ single crystals investigated by measuring the resistive transition at high magnetic fields up to 60 T. In contrast to the strong upturn curvature of $H_{c2}^c(T)$ reported earlier in $\text{NdFeAsO}_{1-x}\text{F}_x$ single crystal, $H_{c2}^c(T)$'s in both of our crystals increase linearly with decreasing temperature near T_c and tends to be saturated at low-enough temperatures. We confirm that the temperature dependences of $H_{c2}^c(T)$'s well follow the two-gap dirty-limit prediction while they deviate from the one-gap WHH prediction, regardless of inclusion of the spin-paramagnetic effect. On the other hand, $H_{c2}^{ab}(T)$ of our crystals show the downturn curvature, consistent with the earlier observation in $\text{NdFeAsO}_{1-x}\text{F}_x$ single crystal and AEFe_2As_2 compounds. The importance of paramagnetic effect on the downturn curvature in $H_{c2}^{ab}(T)$ has already been pointed out for $\text{NdFeAsO}_{1-x}\text{F}_x$ single crystal and AEFe_2As_2 compounds but $H_{c2}^{ab}(T)$ data were analyzed only within the two-gap model.^{9–11,16} In this study, the temperature dependences of $H_{c2}^{ab}(T)$'s are analyzed in terms of two-gap model and the WHH theory including the paramagnetic effect. Our analysis clearly indicates that the flattening of $H_{c2}^{ab}(T)$ is governed mainly by the paramagnetic pair-breaking effect rather than the two-gap effect. This study shows that the upper

critical field in Sm-based iron pnictides is determined by the complex interplay of a two-band nature and the paramagnetic effect depending on the direction of magnetic field application with respect to the crystal axes. We believe this is the generic characteristics of different families of iron-pnictide compounds.

ACKNOWLEDGMENTS

This work was supported by the Korea Science and Engineering Foundation through Acceleration Research Grant No. R17-2008-007-01001-0 and by POSCO. J.S.K. is supported by the POSTECH Research funding.

*Corresponding author; hjlee@postech.ac.kr

- ¹Y. Kamihara, T. Watanabe, M. Hirano, and H. Hosono, *J. Am. Chem. Soc.* **130**, 3296 (2008).
- ²F. Hunte, J. Jaroszynski, A. Gurevich, D. C. Larbalestier, R. Jin, A. S. Sefat, M. A. McGuire, B. C. Sales, D. K. Christen, and D. Mandrus, *Nature* **453**, 903 (2008).
- ³Y. J. Jo, J. Jaroszynski, A. Yamamoto, A. Gurevich, S. C. Riggs, G. S. Boebinger, D. Larbalestier, H. H. Wen, N. D. Zhigadlo, S. Katrych, Z. Bukowski, J. Karpinski, R. H. Liu, H. Chen, X. H. Chen, and L. Balicas, *Physica C* **469**, 566 (2009).
- ⁴M. Rotter, M. Tegel, and D. Johrendt, *Phys. Rev. Lett.* **101**, 107006 (2008).
- ⁵N. Ni, S. L. Bud'ko, A. Kreyssig, S. Nandi, G. E. Rustan, A. I. Goldman, S. Gupta, J. D. Corbett, A. Kracher, and P. C. Canfield, *Phys. Rev. B* **78**, 014507 (2008).
- ⁶K. Sasmal, B. Lv, B. Lorenz, A. M. Guloy, F. Chen, Y. Y. Xue, and C. W. Chu, *Phys. Rev. Lett.* **101**, 107007 (2008).
- ⁷M. M. Altarawneh, K. Collar, C. H. Mielke, N. Ni, S. L. Bud'ko, and P. C. Canfield, *Phys. Rev. B* **78**, 220505(R) (2008).
- ⁸A. Yamamoto, J. Jaroszynski, C. Tarantini, L. Balicas, J. Jiang, A. Gurevich, D. C. Larbalestier, R. Jin, A. S. Sefat, M. A. McGuire, B. C. Sales, D. K. Christen, and D. Mandrus, *Appl. Phys. Lett.* **94**, 062511 (2009).
- ⁹S. A. Baily, Y. Kohama, H. Hiratsmu, B. Maiorov, F. F. Balakirev, M. Hirano, and H. Hosono, *Phys. Rev. Lett.* **102**, 117004 (2009).
- ¹⁰H. Q. Yuan, J. Singleton, F. F. Balakirev, S. A. Baily, G. F. Chen, J. L. Luo, and N. L. Wang, *Nature (London)* **457**, 565 (2009).
- ¹¹M. Kano, Y. Kohama, D. Graf, F. F. Balakirev, A. S. Sefat, M. A. McGuire, B. C. Sales, D. Mandrus, and S. W. Tozer, *J. Phys. Soc. Jpn.* **78**, 084719 (2009).
- ¹²N. D. Zhigadlo, S. Katrych, Z. Bukowski, S. Weyeneth, R. Puzniak, and J. Karpinski, *J. Phys.: Condens. Matter* **20**, 342202 (2008).
- ¹³R. Prozorov, M. E. Tillman, E. D. Mun, and P. C. Canfield, *New J. Phys.* **11**, 035004 (2009).
- ¹⁴Y. Jia, P. Cheng, L. Fang, H. Luo, H. Yang, C. Ren, L. Shan, C. Gu, and H.-H. Wen, *Appl. Phys. Lett.* **93**, 032503 (2008).
- ¹⁵J. Karpinski, N. D. Zhigadlo, S. Katrych, Z. Bukowski, P. Moll, S. Weyeneth, H. Keller, R. Puzniak, M. Tortello, D. Daghero, R. Gonnelli, I. Maggio-Aprile, Y. Fasano, O. Fischer, and B. Batlogg, *Physica C* **469**, 370 (2009).
- ¹⁶J. Jaroszynski, F. Hunte, L. Balicas, Youn-jung Jo, I. Raičević, A. Gurevich, D. C. Larbalestier, F. F. Balakirev, L. Fang, P. Cheng, Y. Jia, and H. H. Wen, *Phys. Rev. B* **78**, 174523 (2008).
- ¹⁷H.-S. Lee, J.-H. Park, J.-Y. Lee, J.-Y. Kim, N.-H. Sung, T.-Y. Koo, B. K. Cho, C.-U. Jung, S. Saini, S.-J. Kim, and H.-J. Lee, *Supercond. Sci. Technol.* **22**, 075023 (2009).
- ¹⁸Y. Jia, P. Cheng, L. Fang, H. Yang, C. Ren, L. Shan, C.-Z. Gu, and H.-H. Wen, *Supercond. Sci. Technol.* **21**, 105018 (2008).
- ¹⁹J. Yang, Z.-A. Ren, G.-C. Che, W. Lu, X.-L. Shen, Z.-C. Li, W. Yi, X.-L. Dong, L.-L. Sun, F. Zhou, and Z.-X. Zhao, *Supercond. Sci. Technol.* **22**, 025004 (2009).
- ²⁰A. K. Pradhan, M. Muralidhar, Y. Feng, M. Murakami, K. Nakao, and N. Koshizuka, *Phys. Rev. B* **64**, 172505 (2001).
- ²¹H. Safar, P. L. Gammel, D. A. Huse, D. J. Bishop, W. C. Lee, J. Giapintzakis, and D. M. Ginsberg, *Phys. Rev. Lett.* **70**, 3800 (1993).
- ²²J. A. Fendrich, W. K. Kwok, J. Giapintzakis, C. J. van der Beek, V. M. Vinokur, S. Fleshler, U. Welp, H. K. Viswanathan, and G. W. Crabtree, *Phys. Rev. Lett.* **74**, 1210 (1995).
- ²³D. Lopez, L. Krusin-Elbaum, H. Safar, E. Righi, F. de la Cruz, S. Grigera, C. Feild, W. K. Kwok, L. Paulius, and G. W. Crabtree, *Phys. Rev. Lett.* **80**, 1070 (1998).
- ²⁴M.-O. Mun, S.-I. Lee, W. C. Lee, P. C. Canfield, B. K. Cho, and D. C. Johnston, *Phys. Rev. Lett.* **76**, 2790 (1996).
- ²⁵D. S. Fisher, M. P. A. Fisher, and D. A. Huse, *Phys. Rev. B* **43**, 130 (1991).
- ²⁶Z. Pribulova, T. Klein, J. Kacmarcik, C. Marcenat, M. Konczykowski, S. L. Bud'ko, M. Tillman, and P. C. Canfield, *Phys. Rev. B* **79**, 020508(R) (2009).
- ²⁷H.-S. Lee *et al.* (unpublished).
- ²⁸Y. Ando, G. S. Boebinger, A. Passner, L. F. Schneemeyer, T. Kimura, M. Okuya, S. Watauchi, J. Shimoyama, K. Kishio, K. Tamasaku, N. Ichikawa, and S. Uchida, *Phys. Rev. B* **60**, 12475 (1999).
- ²⁹U. Welp, W. K. Kwok, G. W. Crabtree, K. G. Vandervoort, and J. Z. Liu, *Phys. Rev. Lett.* **62**, 1908 (1989).
- ³⁰P. Fournier and R. L. Greene, *Phys. Rev. B* **68**, 094507 (2003).
- ³¹I. W. Sumarlin, S. Skanthakumar, J. W. Lynn, J. L. Peng, Z. Y. Li, W. Jiang, and R. L. Greene, *Phys. Rev. Lett.* **68**, 2228 (1992).
- ³²S. I. Vedenev, A. G. M. Jansen, E. Haanappel, and P. Wyder, *Phys. Rev. B* **60**, 12467 (1999).
- ³³J. Jaroszynski, Scott C., Riggs, F. Hunte, A. Gurevich, D. C. Larbalestier, G. S. Boebinger, F. F. Balakirev, Albert Migliori, Z. A. Ren, W. Lu, J. Yang, X. L. Shen, X. L. Dong, Z. X. Zhao, R. Jin, A. S. Sefat, M. A. McGuire, B. C. Sales, D. K. Christen, and D. Mandrus, *Phys. Rev. B* **78**, 064511 (2008).
- ³⁴N. Werthamer, E. Helfand, and P. Hohenberg, *Phys. Rev.* **147**, 295 (1966).
- ³⁵G. Fuchs, S.-L. Drechsler, N. Kozlova, M. Bartkowiak, J. E. Hamann-Borrero, G. Behr, K. Nenkov, H.-H. Klauss, H. Maeter, A. Amato, H. Luetkens, A. Kwadrin, R. Khasanov, J. Freudenberger, A. Köhler, M. Knupfer, E. Arushanov, H. Rosner, B. Büchner, and L. Schultz, *New J. Phys.* **11**, 075007 (2009); G. Fuchs, S.-L. Drechsler, N. Kozlova, G. Behr, A. Köhler, J. Werner, K. Nenkov, R. Klingeler, J. Hamann-Borrero, C. Hess,

- A. Kondrat, M. Grobosch, A. Narduzzo, M. Knupfer, J. Freudenberger, B. Büchner, and L. Schultz, *Phys. Rev. Lett.* **101**, 237003 (2008).
- ³⁶A. M. Clogston, *Phys. Rev. Lett.* **9**, 266 (1962); B. S. Chandrasekhar, *Appl. Phys. Lett.* **1**, 7 (1962).
- ³⁷S.-L. Drechsler, M. Grobosch, K. Koepf, G. Behr, A. Kohler, J. Werner, A. Kondrat, N. Leps, C. Hess, R. Klingeler, R. Schuster, B. Buchner, and M. Knupfer, *Phys. Rev. Lett.* **101**, 257004 (2008).
- ³⁸I. I. Mazin, D. J. Singh, M. D. Johannes, and M. H. Du, *Phys. Rev. Lett.* **101**, 057003 (2008).
- ³⁹Z.-J. Yao, J.-X. Liand, and Z. D. Wang, *New J. Phys.* **11**, 025009 (2009).
- ⁴⁰J. Li and Y. P. Wang, *Chin. Phys. Lett.* **25**, 2232 (2008).
- ⁴¹F. Marsiglio and J. E. Hirsch, *Physica C* **468**, 1047 (2008).
- ⁴²Q. Han, Y. Chen, and Z. D. Wang, *EPL* **82**, 37007 (2008).
- ⁴³A. Gurevich, *Phys. Rev. B* **67**, 184515 (2003).
- ⁴⁴D. J. Singh and M.-H. Du, *Phys. Rev. Lett.* **100**, 237003 (2008).
- ⁴⁵J. R. Shrieffer and J. S. Brooks, *Handbook of High-Temperature Superconductivity* (Springer, New York, 2006).
- ⁴⁶S. I. Vedenev, Cyril Proust, V. P. Mineev, M. Nardone, and G. L. J. A. Rikken, *Phys. Rev. B* **73**, 014528 (2006).
- ⁴⁷Pengcheng Li, F. F. Balakirev, and R. L. Greene, *Phys. Rev. B* **75**, 172508 (2007).
- ⁴⁸J. Singleton and C. Mielke, *Contemp. Phys.* **43**, 63 (2002).
- ⁴⁹M. S. Nam, J. A. Symington, J. Singleton, S. J. Blundell, A. Ardavan, J. A. A. J. Perenboom, M. Kurmoo, and P. Dayk, *J. Phys.: Condens. Matter* **11**, L477 (1999).
- ⁵⁰J. Singleton, P. A. Goddard, A. Ardavan, A. I. Coldea, S. J. Blundell, R. D. McDonald, S. Tozer, and J. A. Schlueter, *Phys. Rev. Lett.* **99**, 027004 (2007).
- ⁵¹S. Weyeneth, R. Puzniak, U. Mosele, N. D. Zhigadlo, S. Katrych, Z. Bukowski, J. Karpinski, S. Kohout, J. Roos, and H. Keller, *J. Supercond. Novel Magn.* **22**, 325 (2009).
- ⁵²S. Weyeneth, R. Puzniak, N. D. Zhigadlo, S. Katrych, Z. Bukowski, J. Karpinski, and H. Keller, *J. Supercond. Novel Magn.* **22**, 347 (2009).
- ⁵³The relatively small anisotropy of our single crystals and the decrease in γ with decreasing temperature ensure a sufficiently uniform current distribution along the c axis in our measurement configurations. The nonuniform current distribution with measurement contacts on the crystal surface, often encountered in highly anisotropic layered materials such as Bi-based cuprates with $\gamma \sim 200$, is significantly reduced in our single crystals. Thus, any artifact introduced to $H_{c2}^c(T)$ can be ruled out.